UC Berkeley
UC Berkeley Previously Published Works

Title
Measurements of the sum of HO2NO2 and CH3O2NO2 in the remote troposphere

Permalink
https://escholarship.org/uc/item/9w65p146

Authors
Murphy, J G
Thornton, J A
Wooldridge, P J
et al.

Publication Date
2004-02-01

Peer reviewed

**Atmospheric
Chemistry
and Physics**

Measurements of the sum of HO_2NO_2 and $CH_3O_2NO_2$ in the remote troposphere

J. G. Murphy[1], **J. A. Thornton**[1*], **P. J. Wooldridge**[1], **D. A. Day**[1], **R. S. Rosen**[1], **C. Cantrell**[2], **R. E. Shetter**[2], **B. Lefer**[2], **and R. C. Cohen**[1,3,4]

[1]University of California at Berkeley, Department of Chemistry, Berkeley, CA, USA
[2]National Center for Atmospheric Research, Atmospheric Chemistry Division, Boulder, CO, USA
[3]University of California at Berkeley, Department of Earth and Planetary Science, Berkeley, CA, USA
[4]Lawrence Berkeley National Laboratory, Division of Energy and Environment Technologies, Berkeley, CA, USA
[*]now at: University of Toronto, Department of Chemistry, Toronto, ON, Canada

Abstract. The chemistry of peroxynitric acid (HO_2NO_2) and methyl peroxynitrate ($CH_3O_2NO_2$) is predicted to be particularly important in the upper troposphere where temperatures are frequently low enough that these compounds do not rapidly decompose. At temperatures below 240 K, we calculate that about 20% of NO_y in the mid- and high-latitude upper troposphere is HO_2NO_2. Under these conditions, the reaction of OH with HO_2NO_2 is estimated to account for as much as one third of the permanent loss of hydrogen radicals. During the Tropospheric Ozone Production about the Spring Equinox (TOPSE) campaign, we used thermal dissociation laser-induced fluorescence (TD-LIF) to measure the sum of peroxynitrates ($\Sigma PNs \equiv HO_2NO_2 + CH_3O_2NO_2 + PAN + PPN + \ldots$) aboard the NCAR C-130 research aircraft. We infer the sum of HO_2NO_2 and $CH_3O_2NO_2$ as the difference between ΣPN measurements and gas chromatographic measurements of the two major peroxy acyl nitrates, peroxy acetyl nitrate (PAN) and peroxy propionyl nitrate (PPN). Comparison with NO_y and other nitrogen oxide measurements confirms the importance of HO_2NO_2 and $CH_3O_2NO_2$ to the reactive nitrogen budget and shows that current thinking about the chemistry of these species is approximately correct. During the spring high latitude conditions sampled during the TOPSE experiment, the model predictions of the contribution of ($HO_2NO_2 + CH_3O_2NO_2$) to NO_y are highly temperature dependent: on average 30% of NO_y at 230 K, 15% of NO_y at 240 K, and <5% of NO_y above 250 K. The temperature dependence of the inferred concentrations corroborates the contribution of overtone photolysis to the photochemistry of peroxynitric acid. A model that includes IR photolysis ($J = 1 \times 10^{-5}\,s^{-1}$) agreed with the observed sum of $HO_2NO_2 + CH_3O_2NO_2$ to better than 35% below 240 K where the concentration of these species is largest.

1 Introduction

Reactions of hydrogen radicals ($HO_x \equiv OH + HO_2$, and RO_2) and nitrogen radicals ($NO_x \equiv NO + NO_2$) affect atmospheric composition and climate by regulating global tropospheric ozone and the Earth's oxidative capacity. Peroxynitrates (RO_2NO_2) link these chemical families, thereby influencing tropospheric ozone production and the abundance of OH in both the troposphere and stratosphere. Non-acyl peroxynitrates such as HO_2NO_2 and $CH_3O_2NO_2$ are increasingly important at temperatures below 240 K, because the molecules are very weakly bound ($\sim$95 kJ/mol) and rapidly dissociate at higher temperature. Consequently these molecules are most important in the stratosphere and upper troposphere.

Knowledge of the chemistry of alkyl RO_2NO_2 species is limited because they are difficult to isolate in the laboratory or to observe directly in the atmosphere. Remote sensing measurements of peroxynitric acid concentrations in the stratosphere show that HO_2NO_2 mixing ratios peak at approximately 200 ppt near 27 km altitude (Rinsland et al., 1986; Rinsland et al., 1996; Sen et al., 1998). The only other measurements are from the Antarctic surface where Slusher et al. (2001) used chemical ionization mass spectrometry to observe HO_2NO_2 mixing ratios on the order of 20 ppt, showing they were nearly equal to nitric acid mixing ratios. Recent OH and HO_2 measurements made in the lower stratosphere at high solar zenith angles (SZA) indicate that there is a source of HO_x that dissociates following absorption of low energy photons (Salawitch et al., 1994; Wennberg et al., 1999). Overtone photodissociation of HO_2NO_2, as

suggested by Donaldson et al. (1997), can explain part of the HO_x source required to account for these observations and some of the temporal variability seen in remote sensing of HO_2NO_2 (Salawitch et al., 2002). These observations and calculations of HO_2NO_2 abundances and their effect on stratospheric HO_x have been the impetus for revisiting the long-wavelength photolysis and kinetics of peroxynitrates in the laboratory (Knight et al., 2002; Roehl et al., 2002; Zhang et al., 2000).

Here we describe the first in situ measurements of these peroxynitrates in the free troposphere. The measurements were made during the Tropospheric Ozone Production about the Spring Equinox (TOPSE) experiment (Atlas et al., 2003). TOPSE flights focused on tropospheric sampling over mid- to high-latitude continental North America during the winter and spring of 2000. Data used in this paper are limited to latitudes north of 50° N and altitudes above 500 m to avoid the effects of recent surface emissions or losses. The data were collected during the daytime at temperatures between 220 and 290 K. Analysis along chemical coordinates (Cohen et al., 2000), in this case temperature and NO_2, and consideration of the NO_y budget are used to evaluate current understanding of photolytic and thermal decomposition rates of HO_2NO_2 and $CH_3O_2NO_2$.

2 Instrumentation

NO_y and its components were measured from the NCAR C-130 aircraft during the TOPSE experiment. Ridley et al. (2000) measured NO, NO_2 and NO_y by conversion to NO followed by O_3+NO chemiluminescence. The NO_2 measurements were precise to ± 4 ppt and accurate to 5%. C_1–C_4 alkyl nitrates (ΣANs) were quantified by GC analysis of whole air samples (Blake et al., 2003). In our analysis, the sum of C_1–C_4 alkyl nitrate observations was linearly interpolated to a 1 min time base. Nitric acid was measured using a mist chamber followed by ion chromatography (Talbot et al., 1990). PAN and PPN were measured in situ by the NCAR Gas Chromatography with Electron Capture Detection (GC-ECD) instrument. The PAN and PPN measurements represent 1–3 s samples with a precision of ± 5 ppt at 20 ppt, ± 3 ppt at 100 ppt, ± 5–7 ppt at 500 ppt. The accuracy of the PAN and PPN measurements is 10%. Because the PAN and PPN measurements were made with the same instrument, we assume their uncertainties are correlated, that is, if necessary, both could be brought to the "true" value by multiplying by a single constant. During a five minute interval, two PAN measurements and one of PPN are obtained.

A two-channel thermal dissociation laser-induced fluorescence (TD-LIF) instrument was used for observations of total peroxynitrates (ΣPNs$\equiv$PAN+PPN+ HO_2NO_2+$CH_3O_2NO_2$+...) and of NO_2. TD-LIF is described in detail in Day et al. (2002). The specific instrument configuration used during TOPSE is described in detail by

Thornton (2002). Briefly, TD-LIF relies on a heated inlet (50 ms residence time at 180°C) to dissociate RO_2NO_2 to yield NO_2 and RO_2. The resultant NO_2 is quantified along with ambient NO_2 using laser-induced fluorescence (LIF). By operating the heated inlet in parallel with an inlet maintained at ambient temperature, ΣPN mixing ratios can be derived from the difference between the NO_2 signals of the two channels. In addition to acyl and non-acyl peroxynitrates, N_2O_5 will also dissociate in the heated inlet, though we expect it was removed through contact with the walls prior to the heated portion of the inlet, and made a negligible contribution to NO_y in the low NO_x conditions sampled during TOPSE. NO_y species such as alkyl nitrates and nitric acid have significantly higher O-NO_2 bond energies than peroxynitrates and would not have dissociated under the inlet conditions used.

The first third of the campaign was used to test and improve some aspects of instrument performance. High time resolution measurements of NO_2 (channel 1) and ΣPNs (channel 2–channel 1) were obtained simultaneously and continuously during the final nineteen flights of the TOPSE experiment. The precision of the measurements for a 1 min average in each channel under optimal conditions was ± 20 ppt which is dominated by uncertainty in the instrument zero. Under some conditions, usually after steep altitude changes, the apparent precision is ± 50 ppt. The precision of ΣPNs is given by:

$$\sigma(\Sigma PNs) = [(\sigma_{channel\,1})^2 + (\sigma_{channel\,2})^2]^{1/2} \qquad (1)$$

and for a typical scenario $\sigma(\Sigma PNs)$ is ± 28 ppt for 1 min averaging. The accuracy of channel 1 is estimated to be 10% and the accuracy of channel 2 to be 15%. The accuracy of the ΣPNs is estimated to be 15% since the accuracy of the two channels is largely correlated and most of the signal is in channel 2. While TD-LIF NO_2 measurements were used for calculating ΣPN, in the model calculations below we use the NCAR photolysis-chemiluminescence measurements of NO_2 because of their superior precision in the low concentration ranges encountered during TOPSE. TD-LIF measurements were, on average, 20 ppt higher than chemiluminescence measurements of NO_2, but the ΣPN measurements are the difference between two channels, and observations with the inlet heater turned off confirm that both channels measure the same amount of NO_2.

Measurements suggest that PAN is the dominant contribution to ΣPNs and that PPN is the only other major acyl peroxynitrate in the air sampled during TOPSE. In order to infer abundances of non-acyl peroxynitrates (hereafter referred to as ΔPNs) we subtract speciated measurements of PAN and PPN obtained by the NCAR GC-ECD instrument from the TD-LIF measurements of ΣPNs.

$$\Delta PNs = \Sigma PNs - PAN - PPN \qquad (2)$$

We averaged 1 min of TD-LIF data about each PAN measurement and interpolated PPN to generate a dataset of all species coincident in time at 1 min resolution.

The uncertainty in ΔPNs has components associated with both the precision and accuracy of the TD-LIF and GC measurements. In what follows, we do not draw any conclusions based on individual measurements, rather our conclusions are based on averages over a large enough sample that uncertainty in mean quantities is entirely a function of the instruments' accuracies. The techniques are thought to be accurate to 10% (GC) and 15% (LIF) and for both techniques one single multiplicative correction (if it could be known) would bring the observed values to the "true" values (to within the precision uncertainty). The accuracy of these instruments depends on a chain of calibration that connects to NIST traceable reference standards of NO or NO$_2$, on the accuracy of flow controllers used to dilute these standards and on titration reactions. None of these factors depend on environmental parameters. Thus the associated accuracy in the average value of a combined quantity like ΔPNs adds in quadrature, since the accuracy of the GC and LIF measurements are assumed to be uncorrelated, resulting in a combined accuracy of 18%. The random error associated with an individual ΔPNs measurement is obtained by standard propagation of error based on Eq. (2);

$$\sigma(\Delta\text{PNs})=[(\sigma_{\Sigma\text{PNs}})^2 + (\sigma_{\text{PAN}})^2 + (\sigma_{\text{PPN}})^2]^{1/2} \quad (3)$$

which results in an uncertainty of $\pm$29 ppt.

In contrast to the expectations outlined above, Fig. 1a shows that the two techniques differ by 35% at high relative humidity and agree at low humidity. In the top panel of Fig. 1, the ratio of ΣPNs/(PAN+PPN) is plotted versus humidity for data that calculations suggest have negligible amounts of ΔPNs (ΔPNs less than 10% of PAN). This figure includes more than half the observations in the dataset. The absolute difference is larger than expected and the accuracy is not observed to be independent of environmental parameters. One or both instruments are not accurate to within the 10 or 15% quoted.

Neither technique is known to have a humidity-dependent bias or interference of this magnitude. We examined a wide range of variables and considered many possible sources of instrument error in the effort to understand the calibration difference between the instruments. Humidity provided the clearest correction. Applying a constraint that

$$\Delta\text{PNs} \geq 0 \quad (4)$$

permits the derivation of a constant that implicitly couples the calibration constants for the two instruments and corrects for this difference as a function of humidity. A correction factor, C=(1+0.0025*%RH), was generated that brings the average (PAN+PPN)/ΣPNs near one when ΔPNs are insignificant. Since we have no reason to apply the correction to one or the other instrument, the TD-LIF data was multiplied by the correction factor C, and the GC data was divided
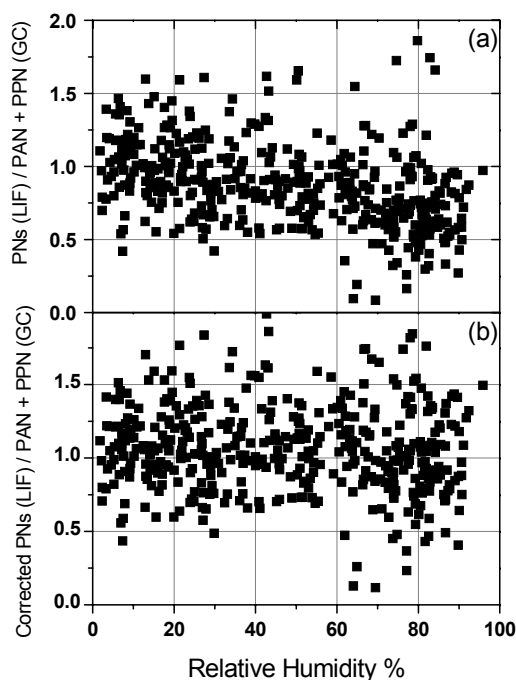

Fig. 1. **(a)** Humidity trend in ratio of LIF to GC measurements where HO$_2$NO$_2$ is predicted be less than 10% of PAN **(b)** Ratio after the humidity-dependent correction has been applied.

by this factor. This removed the humidity bias (Fig. 1b). Throughout the remainder of this paper we use these adjusted datasets. Applying the factor C to the two data sets alters them by 12% on average (+12% ΣPNs and −12% PAN and PPN). The modelled ΔPNs show no trend with relative humidity and the conclusions of this paper would be unchanged if a larger correction had been applied to one or the other instrument. Using Eq. (2) with the corrected datasets provides 1433 1-min measurements of ΔPNs, which calculations suggest are predominantly HO$_2$NO$_2$ and CH$_3$O$_2$NO$_2$. We estimate the uncertainty in ΔPNs is 25%.

Measurements of NO$_y$ and comparison to the sum of individual NO$_y$ compounds (ΣNO$_y$) provide another means to evaluate the relative calibration of the GC-ECD, TD-LIF and NO$_y$ techniques, as well as our ability to infer ΔPNs from the adjusted difference of the two sets of measurements. Figure 2 demonstrates the importance of HO$_2$NO$_2$ in the reactive nitrogen budget and the ability of TD-LIF ΔPN measurements to account for this compound. The ratio ΣNO$_{yi}$/NO$_y$ with the above correction applied to each peroxynitrate dataset, is plotted against fraction of NO$_y$ that is predicted by a model to be HO$_2$NO$_2$. The ratio where ΣNO$_{yi}$=NO$_x$+ΣANs+HNO$_3$+PAN+PPN (gray circle) decreases from a value above 1.1 where ΔPNs are insignificant to close to 0.8 where HO$_2$NO$_2$ contributes a substantial fraction of total NO$_y$. Conversely, the NO$_y$ budget using TD-LIF measurements ΣNO$_{yi}$=NO$_x$+ΣANs+HNO$_3$ + ΣPNs (black square) is approximately a constant 1.2 This suggests that
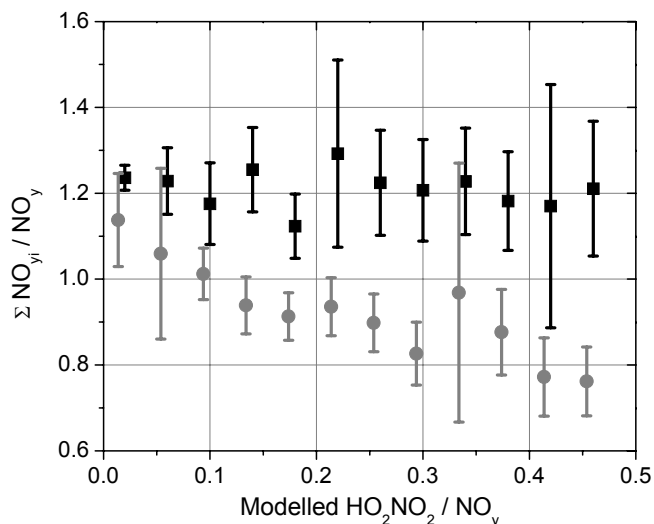
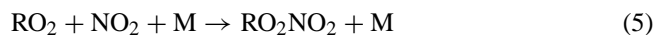**Fig. 2.** $\Sigma NO_{yi}/NO_y$ vs calculated HO_2NO_2/NO_y, using $\Sigma NO_{yi}=$ $NO_x +HNO_3+\Sigma ANs +PAN+PPN$ (●) and $\Sigma NO_{yi} =NO_x+HNO_3$ $+\Sigma ANs+\Sigma PNs$ (■). The data were averaged within $\pm.04$ of HO_2NO_2/NO_y and the error bars represent twice the standard deviation of the mean.

our ΣPN measurements account for the predicted contribution of HO_2NO_2 to the reactive nitrogen budget. If the modelled ΔPNs are added to the PAN and PPN measurements, the average ΣNO_{yi}/total NO_y ratio over the whole campaign is 1.2. If the humidity correction is not applied to the data, the $\Sigma NO_{yi}/NO_y$ ratio using the ΣPN measurements is a constant 1.1, and the ratio using PAN+PPN varies from above 1.2 where ΔPNs are insignificant to 0.8 where ΔPNs are calculated to be 45% of NO_y.

3 Model description and comparison to observations

Peroxynitrates are formed when an RO_2 radical (where R=H, alkyl, or acyl group) reacts with NO_2 (Reaction 5). In the remote atmosphere, HO_2 and CH_3O_2 make up a large fraction of RO_2. Sinks of HO_2NO_2 and $CH_3O_2NO_2$ include thermal decomposition (R6), photolysis (R7), and for HO_2NO_2, reaction with OH (R8). Note that the products given for reaction 8 have not been measured. Models all assume that water is a product of R8 and consequently that R8 is a sink for HO_x radicals.

$$RO_2 + NO_2 + M \rightarrow RO_2NO_2 + M \tag{5}$$

$$RO_2NO_2 + M \rightarrow RO_2 + NO_2 + M \tag{6}$$

$$RO_2NO_2 + h\nu \rightarrow RO_2 + NO_2 \tag{7a}$$

$$or \;\; \rightarrow RO + NO_3 \tag{7b}$$

$$HO_2NO_2 + OH \rightarrow H_2O + NO_2 + O_2 \tag{8}$$
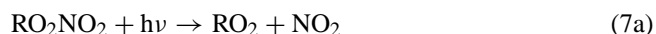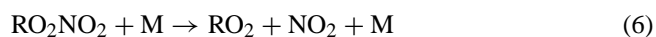
Uncertainties associated with this chemistry are large. For example, for the thermal decomposition of HO_2NO_2 the JPL panel recommends an uncertainty factor of 5 at 298 K and of 13 at 230 K (Sander et al., 2003). Recent laboratory measurements of the UV (Knight et al., 2002) and IR (Roehl et al., 2002) cross sections of peroxynitric acid greatly improve our understanding of its photolysis rate, (J≡R7), although the temperature and pressure dependencies of the quantum yield require further investigation. We know little about the photolysis of $CH_3O_2NO_2$.

We use an instantaneous steady state model representing R5–R8 to predict the abundances of HO_2NO_2 and $CH_3O_2NO_2$.

$$[HO_2NO_2]_{SS}=\frac{k_5[HO_2][NO_2][M]}{k_6[M] + J7 + k_8[OH]} \tag{9}$$

$$[CH_3O_2NO_2]_{SS}=\frac{k_{5'}[CH_3O_2][NO_2][M]}{k_{6'}[M] + J7'} \tag{10}$$

Measurements of NO_2, the spectrally resolved actinic flux, temperature, and pressure are used in the calculations. As a result of the low mixing ratios of NO_2 (50% of the observations have NO_2 below 11 ppt) the precision of the model calculations are roughly proportional to the precision of the NO_2 measurements, for example $\pm40\%$ at 10 ppt NO_2. Although OH and HO_2 were measured during the TOPSE campaign, the observations were too infrequent to use in the model. Steady state concentrations of OH, HO_2, and CH_3O_2 were calculated using the photochemical model described by Cantrell et al. (2003), which included the steady state equations for HO_2NO_2 and $CH_3O_2NO_2$. Four individual calculations in which radicals and reservoirs were solved self-consistently were used to investigate the main sources of uncertainty in the kinetics of HO_2NO_2. Rate constants used in the model are from the JPL-2000 recommendations except for the self-reaction of HO_2 (Christensen et al., 2002) and for the reaction HO_2+O_3 and $OH+O_3$ for which we use JPL-97 recommendations (see Lanzendorf et al., 2001). Photolysis rates were determined using measured actinic flux and made use of the recent molecular data for H_2CO (Smith et al., 2002) and HO_2NO_2 (Knight et al., 2002; Roehl et al., 2002). The UV cross section of $CH_3O_2NO_2$ is assumed to be equal to that of HO_2NO_2. The thermal decomposition of $CH_3O_2NO_2$ dominates down to 220 K, so we need not consider any potential IR overtone photodissociation from the CH groups present in the molecule. In the first calculation (Model A), the IR photolysis rate of HO_2NO_2 is set at 1×10^{-5} s^{-1}, slightly higher than the recommendation of 8.3×10^{-6} s^{-1} from Roehl et al. (2002), which was given for a system with no albedo. In a second calculation (Model B), the IR photolysis rate for HO_2NO_2 was set to zero. In two separate calculations, the rate of thermal decomposition of HO_2NO_2 was varied to the maximum (Model C) and minimum (Model D) limits given in JPL-2003. Model A, with standard thermal decomposition and including IR photolysis,
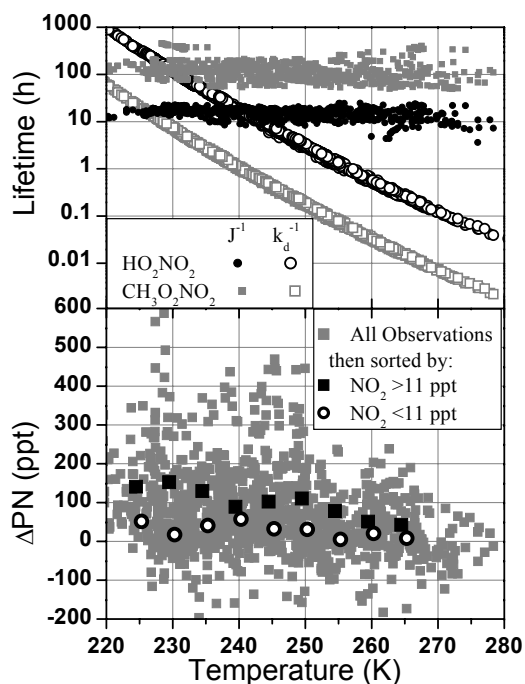
Fig. 3. (upper panel) lifetime of HO$_2$NO$_2$ with respect to thermal decomposition (○) and the sum of photolysis and reaction with OH (●) and of CH$_3$O$_2$NO$_2$ with respect to thermal decomposition (□) and photolysis (■). (lower panel) ΔPN measurements (■) as a function of temperature, averaged into separate temperature bins for NO$_2$ < 11 ppt (○) and for NO$_2$ > 11 ppt (■).

calculates peak HO$_2$NO$_2$ and CH$_3$O$_2$NO$_2$ mixing ratios during the last 19 flights of the TOPSE experiment that range as high as 300 ppt and 100 ppt respectively. It predicts HO$_2$NO$_2$ reaching as much as 50% of measured NO$_y$ and CH$_3$O$_2$NO$_2$ as much as 15% of measured NO$_y$.

Figure 3 depicts the temperature dependence of the thermal and photochemical sinks of these two peroxynitrates. The photochemical sinks (R7 and R8) are nearly independent of temperature. HO$_2$NO$_2$ has a slower thermal decomposition rate and a faster photochemical loss than CH$_3$O$_2$NO$_2$ because of its large infrared photodissociation cross section and because its reaction with OH also contributes to photochemical loss. For HO$_2$NO$_2$, thermal decomposition becomes faster than the photochemical sinks above 240 K, while the crossing point for CH$_3$O$_2$NO$_2$ is near 220 K. One consequence of this is that the lifetime of HO$_2$NO$_2$ (~12 h in sunlit conditions) is independent of temperature for the colder conditions sampled during TOPSE.

The instantaneous steady state model is valid only when the lifetime of the HO$_2$NO$_2$ or CH$_3$O$_2$NO$_2$ is short compared to the rate of change of its sources and sinks. This is not always true for these peroxynitrates under the coldest conditions sampled during TOPSE. However, many of the data points were collected at high latitudes during the late spring, where the photochemistry has a fairly shallow diur-
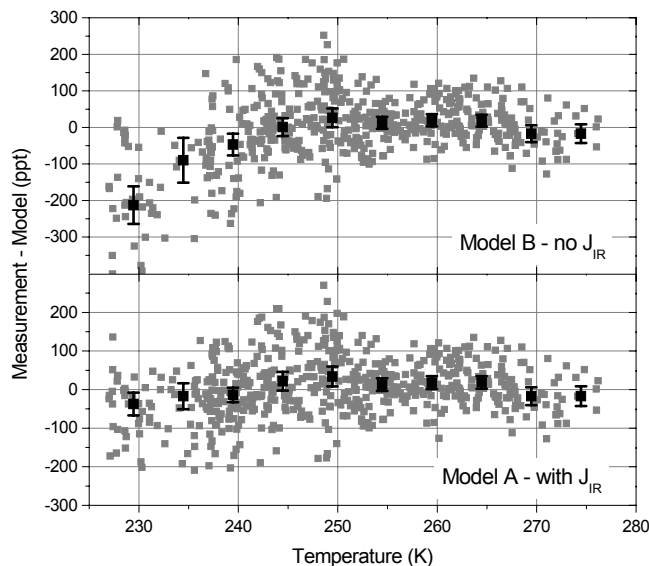

Fig. 4. Difference between measured and modelled ΔPNs for a model without IR photolysis (upper panel) and a model including IR photolysis for HO$_2$NO$_2$ (lower panel). The black squares represent the median of each 5 K bin and the error bars are twice the standard deviation of the mean.

nal profile, making the model steady state predictions reasonable estimates. To help avoid any bias due to being strongly out of steady state, model results in which the lifetime of either compound exceeded twelve hours were discarded, unless there were more than 20 hours of sunlight per day at that location.

In the lower panel of Fig. 3, the ΔPN concentrations inferred from our observations are displayed versus temperature. The mixing ratios below approximately 250 K are larger than at warmer temperatures. The wide range of concentrations at each temperature derives partly from variation in the abundance of HO$_2$, CH$_3$O$_2$ and NO$_2$ radicals in the airmass. As an example, the large symbols are the mean ΔPNs within a 5 K bin for NO$_2$ mixing ratios above (black squares) and below (open circles) 11 ppt, which was the median NO$_2$ during the last 19 flights of TOPSE. On average, higher values of ΔPNs were observed when NO$_2$ mixing ratios were higher than average and vice versa. In addition to being proportional to NO$_2$, below 250 K ΔPNs are calculated to depend strongly on the IR photolysis of HO$_2$NO$_2$, which has only recently been recognized as large enough to affect its atmospheric mixing ratio. Our data provides direct observational evidence for this term. In the upper panel of Fig. 4 we show the difference between the ΔPN observations and model B (no IR photolysis) and in the lower panel we show the difference between ΔPNs and model A. The relative significance of IR photolysis increases strongly as a function of decreasing temperature and dominates over thermal decomposition as a sink of HO$_2$NO$_2$ below 235 K. At 230 K, the model without IR
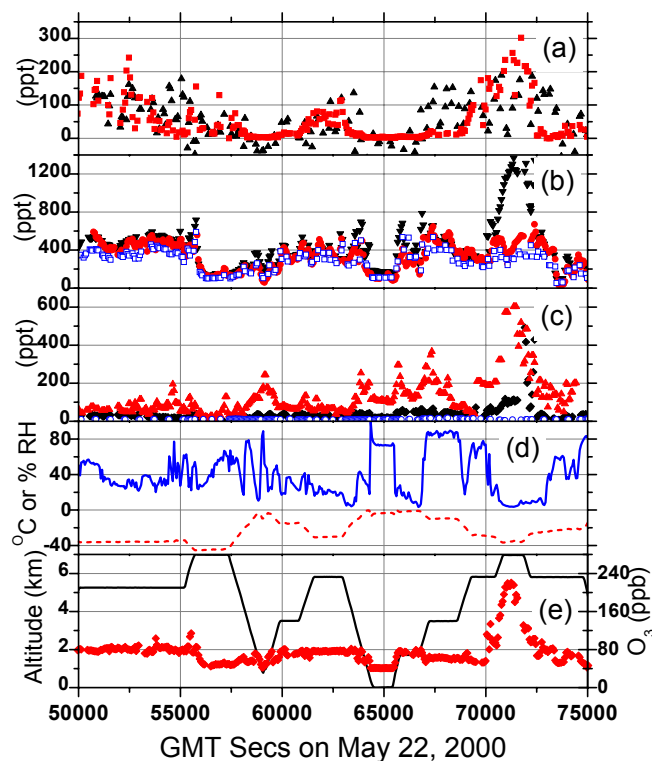
Fig. 5. Observations during a flight between Thule and Winnipeg on 22 May 2000 **(a)** ΔPN measurements (▲) and predictions from Model A (■) **(b)** NO_y (▼), PAN+PPN (□), $\sum PN$ (●) **(c)** HNO_3 (▲), NO_x (◇), $\sum ANs$ (○) **(d)** temperature (- -), % relative humidity (–) **(e)** altitude (–), O_3 (◇).

Fig. 6. Comparison of average ΔPN observations and Model A predictions with the error bars representing twice the standard deviation on the mean and a 1:1 line shown.

photolysis has, on average, 200 ppt more HO_2NO_2 than the observed ΔPNs. There are specific events where modeled ΔPNs exceed the measurements by 400 ppt without the infrared sink of HO_2NO_2.

The model A peroxynitrate ($HO_2NO_2+CH_3O_2NO_2$) predictions are compared to ΔPN measurements in a time series during a TOPSE flight on May 22 (Fig. 5 upper panel). This flight between Thule and Winnipeg sampled a wide range of tropospheric conditions and encountered air of mixed stratospheric-tropospheric character ($O_3 > 100$ ppb) near the end of the flight. HNO_3 and NO_x make significant contributions to NO_y in this particular airmass, which nonetheless has quite high PAN mixing ratios. The ΔPN measurements are generally scattered around the model predictions and tend to be highest under the coldest conditions as expected based on the chemistry described above. During this flight, NO_x and ΔPNs are nearly equal.

The figures above show that ΔPNs vary as expected in response to two of the individual terms in the steady-state equations (J and NO_2) and vary along a flight track as the steady state calculation suggests they should.
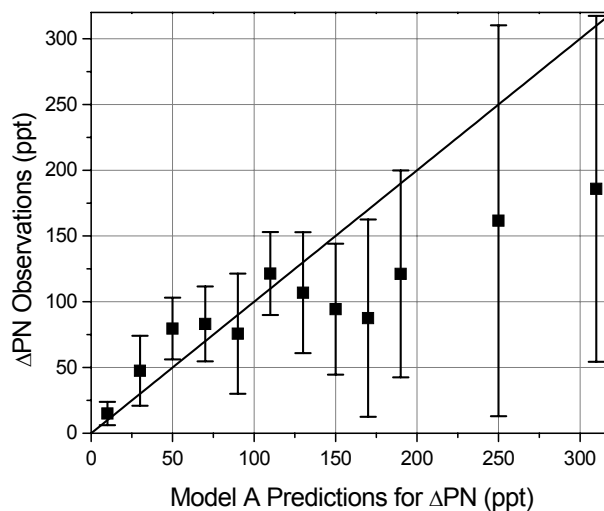
Table 1 compiles the median contribution of each species or group to the NO_y budget during TOPSE for temperatures above and below 240 K. Peroxynitrates were the most significant fraction of NO_y under all temperature regimes sampled during TOPSE. The ΔPN predictions of Model A and Model B are shown for reference to the observations inferred by $\sum PNs-(PAN+PPN)$. The significance of ΔPNs to NO_y predicted by Model A and observed agree to within a factor of 2 above 240 K and to within 35% below 240 K. The ratio $\sum NO_{yi}/NO_y$ is between 1.1 and 1.25 using either TD-LIF $\sum PNs$ or GC-ECD PAN+PPN and modelled ΔPNs.

Figure 6 shows a direct comparison of calculations of ΔPNs and the observations for all flights in the analysis. Within the statistical variance, the observations and model agree. However model predictions exceed the observations at higher mixing ratios and the fact that nearly all calculated concentrations above 150 ppt are higher than observations suggests the effect is statistically reliable. If the steady state approximation is correct, then this could indicate an error in the photochemistry of HO_2NO_2 or the thermal decomposition of $CH_3O_2NO_2$. We investigated the factor of 5–15 uncertainty in the HO_2NO_2 thermal decomposition rate at temperatures in the 220–298 K range. Model calculations (C,D) that incorporated the most extreme values for rates of thermal decomposition predicted ΔPN concentrations that differed at most by 100 ppt, with the greatest effect occurring between 235 and 250 K. Both models were less consistent with the observations than Model A, but because HO_2NO_2 is largest where thermal decomposition is slow compared to photolysis we are unable to define substantially more precise limits on the rate of thermal decomposition than recommended by the JPL panel. We examined other possible effects but found no single explanation that would bring the model-measurement comparison into significantly better agreement.

Table 1. NO$_y$ composition (500–8000 m) above and below 240 K during TOPSE flights between 6 April and 23 May 2000.

NO$_{yi}$	T$<$240 K	T$>$240 K
	%NO$_y$	%NO$_y$
$\sum$PNs[a]	90	86
PAN+PPN[b]	73	76
Inferred ΔPNs	17	10
Model A ΔPNs	22	5
Model B ΔPNs	34	5
HNO$_3$	11	25
NO$_x$[c]	5	8
Alkyl Nitrates	4	4
$\sum$NO$_{yi}$	$\sum$NO$_{yi}$/NO$_y$	$\sum$NO$_{yi}$/NO$_y$
(NO$_x$+$\sum$ANs + HNO$_3$+$\sum$PNs)	1.10	1.23
(NO$_x$+$\sum$ANs + HNO$_3$ + PAN + PPN + ModelAΔPNs)	1.15	1.18

[a] TD-LIF measurements with humidity correction applied, [b] GC-ECD measurements with humidity correction applied,
[c] Chemiluminescence measurements

4 Discussion

In the upper troposphere, several studies (Folkins et al., 1997; Jaegle et al., 2000; Jaegle et al., 2001) have described calculations indicating that reaction of OH with HO$_2$NO$_2$ is a dominant sink for HO$_x$. Analysis of HO$_x$ observations by Faloona et al. (2000) suggest that a model in which the HO$_2$NO$_2$ equilibrium constant is reduced by a factor of five, or with HO$_2$NO$_2$ formation suppressed entirely, provides a more accurate representation of upper tropospheric HO$_x$ observations than the standard model. We estimate that inclusion of the IR photolysis of HO$_2$NO$_2$ should have nearly the same effect on HO$_2$NO$_2$ concentrations at the altitudes where most of the observations described by Faloona et al. (2000) were collected. The main consequence is a decrease in the modelled abundance of HO$_2$NO$_2$. However, the IR photolysis will have a distinctly different temperature dependence than the suggested change to the equilibrium constant. For the coldest conditions sampled during TOPSE, between 220 K and 240 K, Model A, which includes IR photolysis, predicts $\sim$10% more HO$_x$ than Model B, and also results in slightly different HO$_x$ partitioning.

Another interesting aspect of HO$_2$NO$_2$ and CH$_3$O$_2$NO$_2$ chemistry is their behavior as a short-term reservoir for HO$_x$ and NO$_x$ radicals. Under sunlit conditions, the radicals and alkyl peroxynitrates should reach steady state, yet once the sun sets, formation diminishes and the only remaining sink is thermal decomposition. During twelve hours of darkness in the upper troposphere at 240 K, all the CH$_3$O$_2$NO$_2$ and over half of the HO$_2$NO$_2$ will have thermally dissociated, releasing on the order of tens to hundreds ppt of CH$_3$O$_2$ and HO$_2$. The fate of these radicals during the night will depend strongly on the abundance of NO$_x$ and O$_3$. This fact underscores the importance of making measurements at night to challenge our understanding of radical sources and sinks.

5 Conclusions

We describe observations of ΔPNs and demonstrate that they are HO$_2$NO$_2$ and CH$_3$O$_2$NO$_2$. The observations show that during the spring high latitude conditions sampled during the TOPSE experiment, the contribution of ΔPNs to NO$_y$ is highly temperature dependent, with ΔPNs on average 30% of NO$_y$ at 230 K and 7% of NO$_y$ at 250 K. The magnitude and observed temperature dependence of the mixing ratios is consistent with recent laboratory evidence that the J value for HO$_2$NO$_2$ has a large IR component. Prior analyses of the NO$_y$ budget in the upper troposphere that did not take into account HO$_2$NO$_2$ or the new J value should be revisited.

References

Atlas, E. L., Ridley, B. A., and Cantrell, C. A.: The Tropospheric Ozone Production about the Spring Equinox (TOPSE) Experiment: Introduction, J. Geophys. Res.-Atmos., 108, 8353, doi:8310.1029/2002JD003172, 2003.

Blake, N. J., Blake, D. R., Sive, B. C., Katzenstein, A. S., Meinardi, S., Wingenter, O. W., Atlas, E. L., Flocke, F., Ridley, B. A., and Rowland, F. S.: The seasonal evolution of NMHCs and light alkyl nitrates at middle to high northern latitudes during TOPSE, J. Geophys. Res.-Atmos., 108, 8359, doi:8310.1029/2001JD001467, 2003.

Cantrell, C. A., Mauldin, L., Zondlo, M., et al.: Steady state free radical budgets and ozone photochemistry

during TOPSE, J. Geophys. Res.-Atmos., 108, 8361, doi:8310.1029/2002JD002198, 2003.

Christensen, L. E., Okumura, M., Sander, S. P., Salawitch, R. J., Toon, G. C., Sen, B., Blavier, J.-F., and Jucks, K. W.: Kinetics of HO$_2$+HO$_2$ to H$_2$O$_2$+O$_2$: Implications for Stratospheric H$_2$O$_2$, Geophys. Res. Lett., 29, 1299, doi:1210.1029/2001GL014525, 2002.

Cohen, R. C., Perkins, K. K., Koch, L. C., Stimpfle, R. M., Wennberg, P. O., Hanisco, T. F., Lanzendorf, E. J., Bonne, G. P., Voss, P. B., Salawitch, R. J., Del Negro, L. A., Wilson, J. C., McElroy, C. T., and Bui, T. P.: Quantitative constraints on the atmospheric chemistry of nitrogen oxides: An analysis along chemical coordinates, J. Geophys. Res.-Atmos., 105, 24 283–24 304, 2000.

Day, D. A., Wooldridge, P. J., Dillon, M. B., Thornton, J. A., and Cohen, R. C.: A thermal dissociation laser-induced fluorescence instrument for in situ detection of NO$_2$, peroxy nitrates, alkyl nitrates, and HNO$_3$, J. Geophys. Res.-Atmos., 107, 4046, doi:4010.1029/2001JD000779, 2002.

Donaldson, D. J., Frost, G. J., Rosenlof, K. H., Tuck, A. F., and Vaida, V.: Atmospheric radical production by excitation of vibrational overtones via absorption of visible light, Geophys. Res. Lett., 24, 2651–2654, 1997.

Faloona, I., Tan, D., Brune, W. H., Jaegle, L., Jacob, D. J., Kondo, Y., Koike, M., Chatfield, R., Pueschel, R., Ferry, G., Sachse, G., Vay, S., Anderson, B., Hannon, J., and Fuelberg, H.: Observations of HO$_x$ and its relationship with NO$_x$ in the upper troposphere during SONEX, J. Geophys. Res.-Atmos., 105, 3771–3783, 2000.

Folkins, I., Wennberg, P. O., Hanisco, T. F., Anderson, J. G., and Salawitch, R. J.: OH, HO$_2$, and NO in two biomass burning plumes: Sources of HO$_x$ and implications for ozone production, Geophys. Res. Lett., 24, 3185–3188, 1997.

Jaegle, L., Jacob, D. J., Brune, W. H., Faloona, I., Tan, D., Heikes, B. G., Kondo, Y., Sachse, G. W., Anderson, B., Gregory, G. L., Singh, H. B., Pueschel, R., Ferry, G., Blake, D. R., and Shetter, R. E.: Photochemistry of HO$_x$ in the upper troposphere at northern midlatitudes, J. Geophys. Res.-Atmos., 105, 3877–3892, 2000.

Jaegle, L., Jacob, D. J., Brune, W. H., and Wennberg, P. O.: Chemistry of HO$_x$ radicals in the upper troposphere, Atmos. Environ., 35, 469–489, 2001.

Knight, G., Ravishankara, A. R., and Burkholder, J. B.: UV absorption cross sections of HO$_2$NO$_2$ between 343 and 273 K, Phys. Chem. Chem. Phys., 4, 1432–1437, 2002.

Lanzendorf, E. J., Hanisco, T. F., Wennberg, P. O., Cohen, R. C., Stimpfle, R. M., and Anderson, J. G.: Comparing atmospheric [HO$_2$]/[OH] to modeled [HO$_2$]/[OH]: Identifying discrepancies with reaction rates, Geophys. Res. Lett., 28, 967–970, 2001.

Ridley, B., Walega, J., Montzka, D., Grahek, F., Atlas, E., Flocke, F., Stroud, V., Deary, J., Gallant, A., Boudries, H., Bottenheim, J., Anlauf, K., Worthy, D., Sumner, A. L., Splawn, B., and Shepson, P.: Is the Arctic surface layer a source and sink of NO$_x$ in winter/spring?, J. Atmos. Chem., 36, 1–22, 2000.

Rinsland, C. P., Gunson, M. R., Salawitch, R. J., Michelsen, H. A., Zander, R., Newchurch, M. J., Abbas, M. M., Abrams, M. C., Manney, G. L., Chang, A. Y., Irion, F. W., Goldman, A., and Mahieu, E.: Atmos/Atlas-3 Measurements of Stratospheric Chlorine and Reactive Nitrogen Partitioning Inside and Outside

the November 1994 Antarctic Vortex, Geophys. Res. Lett., 23, 2365–2368, 1996.

Rinsland, C. P., Zander, R., Farmer, C. B., Norton, R. H., Brown, L. R., Russell, J. M., and Park, J. H.: Evidence for the presence of 802.7 cm^{-1} band Q branch of HO$_2$NO$_2$ in high-resolution solar absorption-spectra of the stratosphere, Geophys. Res. Lett., 13, 761–764, 1986.

Roehl, C. M., Nizkorodov, S. A., Zhang, H., Blake, G. A., and Wennberg, P. O.: Photodissociation of peroxynitric acid in the near-IR, J. Phys. Chem. A., 106, 3766–3772, 2002.

Salawitch, R. J., Wennberg, P. O., Toon, G. C., Sen, B., and Blavier, J. F.: Near IR photolysis of HO$_2$NO$_2$: Implications for HO$_x$, Geophys. Res. Lett., 29, 1762, 1710.1029/2002GL015006, 2002.

Salawitch, R. J., Wofsy, S. C., Wennberg, P. O., Cohen, R. C., Anderson, J. G., Fahey, D. W., Gao, R. S., Keim, E. R., Woodbridge, E. L., Stimpfle, R. M., Koplow, J. P., Kohn, D. W., Webster, C. R., May, R. D., Pfister, L., Gottlieb, E. W., Michelsen, H. A., Yue, G. K., Prather, M. J., Wilson, J. C., Brock, C. A., Jonsson, H. H., Dye, J. E., Baumgardner, D., Proffitt, M. H., Loewenstein, M., Podolske, J. R., Elkins, J. W., Dutton, G. S., Hintsa, E. J., Dessler, A. E., Weinstock, E. M., Kelly, K. K., Boering, K. A., Daube, B. C., Chan, K. R., and Bowen, S. W.: The Diurnal Variation of Hydrogen, Nitrogen, and Chlorine Radicals – Implications For the Heterogeneous Production of HNO$_2$, Geophys. Res. Lett., 21, 2551–2554, 1994.

Sander, S. P., Kurylo, J. M., Orkin, V. L., Golden, D. M., Huie, R. E., Finlayson-Pitts, B. J., Kolb, C. E., Molina, M. J., Friedl, R. R., Ravishankara, A. R., and Moortgat, G. K.: Chemical Kinetics and Photochemical Data for Use in Stratospheric Modeling, Evaluation Number 14, NASA Jet Propulsion Laboratory, California Institute of Technology, Pasadena, CA, 2003.

Sen, B., Toon, G. C., Osterman, G. B., Blavier, J. F., Margitan, J. J., Salawitch, R. J., and Yue, G. K.: Measurements of reactive nitrogen in the stratosphere, J. Geophys. Res.-Atmos., 103, 3571–3585, 1998.

Slusher, D. L., Pitteri, S. J., Haman, B. J., Tanner, D. J., and Huey, L. G.: A chemical ionization technique for measurement of pernitric acid in the upper troposphere and the polar boundary layer, Geophys. Res. Lett., 28, 3875–3878, 2001.

Smith, G. D., Molina, L. T., and Molina, M. J.: Measurement of radical quantum yields from formaldehyde photolysis between 269 and 339 nm, J. Phys. Chem. A., 106, 1233–1240, 2002.

Talbot, R. W., Vijgen, A. S., and Harriss, R. C.: Measuring Tropospheric HNO$_3$ – Problems and Prospects For Nylon Filter and Mist Chamber Techniques, J. Geophys. Res.-Atmos., 95, 7553–7561, 1990.

Thornton, J. A.: Nitrogen Dioxide, Peroxynitrates, and the Chemistry of Tropospheric O$_3$ Production: New Insights from In Situ Measurements, Doctoral thesis, University of California, Berkeley, 2002.

Wennberg, P. O., Salawitch, R. J., Donaldson, D. J., Hanisco, T. F., Lanzendorf, E. J., Perkins, K. K., Lloyd, S. A., Vaida, V., Gao, R. S., Hintsa, E. J., Cohen, R. C., Swartz, W. H., Kusterer, T. L., and Anderson, D. E.: Twilight observations suggest unknown sources of HO$_x$, Geophys. Res. Lett., 26, 1373–1376, 1999.

Zhang, H., Roehl, C. M., Sander, S. P., and Wennberg, P. O.: Intensity of the second and third OH overtones of H$_2$O$_2$, HNO$_3$, and HO$_2$NO$_2$, J. Geophys. Res.-Atmos., 105, 14 593–14 598, 2000.